

Hierarchical excluded volume screening in solutions of bottlebrush polymers

Jarosław Paturej^{1,2*}, Torsten Kreer^{1*}

¹Leibniz-Institut für Polymerforschung Dresden e.V., 01069 Dresden, Germany

²Institute of Physics, University of Szczecin, 70451 Szczecin, Poland

*To whom correspondence should be addressed; E-mail: jpaturej@univ.szczecin.pl

Polymer bottlebrushes provide intriguing features being relevant both in nature and in synthetic systems. While their presence in the articular cartilage optimizes synovial joint lubrication, bottlebrushes offer pathways for fascinating applications, such as within super-soft elastomers or for drug delivery. However, the current theoretical understanding lacks completeness, primarily due to the complicated interplay of many length scales. Herein, we develop an analytical model that demonstrates how structural properties of bottlebrushes depend on the concentration, ranging from dilute solutions to highly concentrated melts. The validity of our model is supported by data from extensive molecular dynamics simulation. We demonstrate that the hierarchical structure of bottlebrushes dictates a sequence of conformational changes as the solution concentration increases. The effect is mediated by screening of excluded volume interactions at subsequent structural parts of the bottlebrushes. Our findings provide important insights that should enable improved customization of novel materials based on the architectural design of polymer bottlebrushes.

Introduction

Bottlebrushes are polymers consisting of linear backbones with densely grafted polymeric side chains [1–4]. Recent progress in polymerization methodologies enables controlled synthesis of these branched macromolecules [5–13]. Attaching side chains to the backbone leads to significant correlation of the backbone monomers due to the steric repulsion between the side chains. The variation of architecture, i.e., length and grafting density of side chains, allows for systematic tuning of molecular conformation and physical properties of bottlebrushes [14]. These unique features make bottlebrushes candidates for diverse applications including super-soft elastomers

[15, 16], drug delivery agents [17], molecular sensors [18], stimuli-responsive [19–21] and protective surfaces [22], emulsifiers [23], lubricants [24], porous [25], self-assembled [26, 27], and thermoplastic [28] materials, photolithography [29], ionic transport [30], photonics [31], and energy storage [32]. In addition, bottlebrush macromolecules are of great importance in biology, since a myriad of bottlebrush-like glycoproteins and proteoglycans regulate crucial functions in the human body including clearance of lungs [33], joint lubrication [34], and cell protection [35].

Given that the properties of bottlebrushes are very distinct in comparison to linear polymers, they have been an active field of exploration for numerous theoretical [36–48], experimental [16, 49–63], and numerical investigations [38, 47, 48, 55, 64–74]. A majority of these studies has focused on basic structural properties in solutions and in the adsorbed state. Nevertheless, even the most simple question of how the size of a bottlebrush in dilute solution depends on architecture parameters is still a matter of debate. Several theoretical approaches have been proposed to address this problem. The main difficulty is the interplay between many length scales characterizing the bottlebrush structure.

Existing analytical theories of bottlebrushes in dilute solution and under good solvent conditions assume stretchable or persistent, rod-like configurations of the backbone at length scales comparable to [36] or larger [39] than the size of side chains and do not include self-consistently the coupling between elasticity of backbone and side chains [36, 39]. The size of the macromolecule predicted from these models scales as $R_0 \propto N_{\text{bb}}^{3/5} N_{\text{sc}}^\alpha$, with α as low as $9/25$ [36, 39] or as high as $3/4$ [39], where N_{bb} and N_{sc} respectively are the degrees of polymerization of backbone and side chains.

The concentration dependence of the macromolecular structure of bottlebrushes has received much less attention. The model of Birshstein *et al.* [36] for bottlebrushes in dilute solutions was used as a starting point for scaling analysis anticipating a sequence of decays in the molecular size with increasing concentration, c [37]. Three different concentration regimes for the size of bottlebrushes are predicted in this study: $R_{\text{I}} \propto c^{-1/8}$ for semi-dilute solutions, $R_{\text{II}} \propto c^{-17/56}$ for larger concentrations, and $R_{\text{III}} \propto c^{-1/8}$ for melts.

A thorough understanding of bottlebrush conformations, in particular under melt conditions,

is vital for the design of novel polymeric materials with superior mechanical properties [16]. Architecture-induced increase of the bottlebrush persistence length is the key feature underlying physical properties of melts and elastomers. Bottlebrushes in a melt behave as flexible filaments, where side chains reduce molecular overlap and suppress entanglements among macromolecules [47]. This results in the modification of dynamical and rheological properties of bulk polymers [15, 16, 75–78] and allows for synthesis of supersoft and superelastic, solvent-free elastomers, with shear moduli down to 100 Pa and tensile strains at break up to 1000% in a solvent free state [16]. However, before the dynamics of bottlebrush polymers can be addressed, a solid theory describing their static properties is highly desirable.

In this work, we present a theoretical approach that allows one to characterize the equilibrium structure of polymers with grafted side chains, covering dilute, semi-dilute, and highly concentrated solutions. Our theoretical findings are compared to data from extensive molecular dynamics (MD) simulations of a coarse-grained bead-spring polymer model. We identify four concentration regimes for the size of bottlebrushes, which gradually establish upon increasing concentration. They follow from a hierarchical screening of excluded volume effects on various length scales. Excluded volume screening first takes place at the largest length scale, along the backbone of the macromolecules, for concentrations slightly above their overlap concentration. In this regime, the size of the macromolecule scales with concentration as $R_1 \propto c^{-1/8}$. Further increase of the concentration leads to screening at length scales comparable to the length of the persistent segment. The latter results from correlation between backbone monomers due to the steric repulsion among adjacent side chains. Here, our theory predicts $R_2 \propto c^{-1/4}$. For even larger concentrations, excluded volume screening occurs along the interpenetrating side chains of different macromolecules, which yields $R_3 \propto c^{-4/13}$. Under melt conditions, limited interpenetration between bottlebrushes favors screening of excluded volume among side chains of the same macromolecule and results in $R_4 \propto c^{-2/5}$.

Our article is organized as follows: In the next section, we discuss conformational properties of bottlebrushes in dilute solutions using a mean field approach. Then, we present results for the concentration dependence of bottlebrush conformations obtained from scaling theory and compare

them to data of our systematic MD simulations. In the last section, we summarize our findings and draw conclusions. The simulation model and the details of our scaling analysis are described in the Methods section.

Results

Dilute solutions of bottlebrushes

The conformation of a bottlebrush macromolecule in dilute solution can be represented as a sequence of cylindrical subsegments, where each cylinder of length $l_0(N_{sc}, z)$ and radius $R_{sc,0}(N_{sc}, z)$ contains $n_0(N_{sc}, z)$ backbone monomers, see Fig. 1. Here, N_{sc} is the number of monomers per side chain and z is the grafting density of side chains. For grafting densities above or equal to unity ($z \geq 1$), z is the number of grafted side chains per backbone monomer. Correspondingly, a value of $z < 1$ means that a side chain is grafted to every $1/z$ -th backbone monomer.

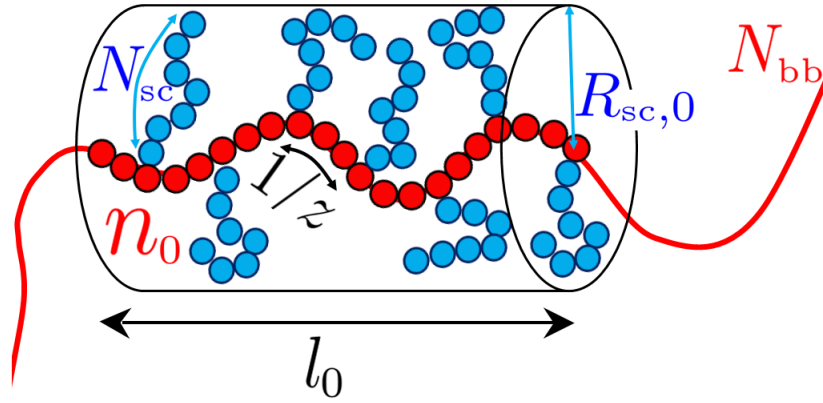


FIG. 1: Molecular architecture of a bottlebrush polymer. The bottlebrush molecule consists of a backbone with N_{bb} monomers (red beads) and side chains (blue beads), which are grafted to every z -th backbone monomer. Each side chain is composed of N_{sc} monomers. The total number of bottlebrush monomers is $N_{bb}(1 + N_{sc}z)$. The bottlebrush molecule can be represented as a chain of effective cylindrical segments. Each segment contains n_0 backbone monomers, has a length l_0 and a radius $R_{sc,0}$.

The cylindrical subsegments can be interpreted as persistent segments, reflecting the coupling between backbone monomers due to the steric repulsion between nearby side chains. The size of a bottlebrush in dilute solution can be estimated from the mean field free energy per cylinder, which

reads

$$F \propto \frac{l_0^2}{n_0} + \frac{R_{sc,0}^2}{N_{sc}} n_0 z + \frac{n_0^2 (1 + N_{sc} z)^2}{l_0 R_{sc,0}^2}. \quad (1)$$

In the above equation, we have neglected numerical pre-factors and set the excluded volume parameter, the thermal energy, and the effective monomer size (or Kuhn length) to unity. Note that backbone and side chains are assumed to be of the same chemical nature.

The first and the second term in Eq. (1) respectively describe the stretching energy of backbone and side chains, while the third term accounts for the overall excluded volume interaction among all monomers within the cylinder. The latter term overestimates the excluded volume interaction as it is commonly done for polymers in good solution [79]. However, previous approaches [38], which utilize similar expressions describing the free energy for the entire macromolecule (and not for a subsegment), invoke an even larger overestimation of the excluded volume interaction.

The free energy of Eq. (1) has to be minimized with respect to both l_0 and $R_{sc,0}$. The derivatives $\frac{\partial}{\partial l_0} F = 0$ and $\frac{\partial}{\partial R_{sc,0}} F = 0$ yield

$$l_0 \propto n_0 R_{sc,0} \sqrt{\frac{z}{N_{sc}}} \quad \text{and} \quad (2)$$

$$R_{sc,0} \propto (1 + N_{sc} z)^{2/5} \left(\frac{N_{sc}}{z} \right)^{3/10}. \quad (3)$$

In Fig. 2, we compare the results of our MD simulations for the mean-square end-to-end distance of side chains, $\langle R_{sc,0}^2 \rangle$, plotted as a function of the scaling variable, $(1 + N_{sc} z)^{4/5} (N_{sc}/z)^{3/5}$, to the prediction of Eq. (3). For large enough values of N_{sc} and z ($N_{sc} z \gtrsim 8$) the theoretically estimated mean-square size of side chains demonstrates perfect agreement with the simulation data. Note that in Fig. 2 and in what follows, all data are presented in Lennard-Jones units (see Methods section for details).

If grafting density and number of side chain monomers are not extremely large, one can assume a semiflexible backbone inside the cylinder [88]. Then, $R_{sc,0}$ is the only length scale that determines the dependence of the persistence length on N_{sc} and z , i.e., $l_0 \propto R_{sc,0}$. This implies that intrinsic rigidity forbids bending of the backbone on length scales smaller than $R_{sc,0}$. From

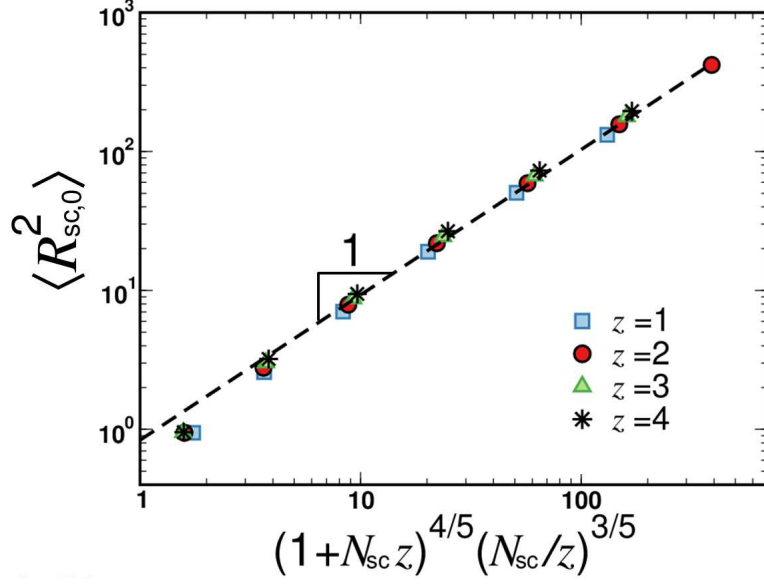


FIG. 2: **Size of bottlebrush side chains in dilute solution.** Mean-square end-to-end distance of side chains, $\langle R_{sc,0}^2 \rangle$, in dilute solution (concentration $c = 10^{-3}$) as a function of the scaling variable, $(1 + N_{sc}z)^{4/5} (N_{sc}/z)^{3/5}$. Data are presented for various grafting densities, z , as indicated in the legend, and fixed degree of polymerization of backbone, $N_{bb} = 100$. The dashed line represents the theoretical prediction of Eq. (3). Error bars for all data points are smaller than symbol size.

Eq. (2), we obtain

$$n_0 \propto \sqrt{\frac{N_{sc}}{z}}, \quad (4)$$

such that Eq. (3) leads to

$$l_0 \propto R_{sc,0} \propto (1 + N_{sc}z)^{2/5} n_0^{3/5}. \quad (5)$$

The latter equation reveals a self-avoiding walk statistics of the backbone monomers inside the cylinder, i.e., $l_0 \propto n_0^{3/5}$ [89]. Correspondingly, the conformation of the bottlebrush as a whole can be regarded as a self-avoiding walk of N_{bb}/n_0 cylindrical segments of length l_0 , where N_{bb} denotes the (total) number of backbone monomers. With Eq. (5), the equilibrium size of a bottlebrush in dilute solution reads

$$R_0 \propto l_0 \left(\frac{N_{bb}}{n_0} \right)^{3/5} \propto (1 + N_{sc}z)^{2/5} N_{bb}^{3/5}. \quad (6)$$

In Fig. 3, simulations results for the re-scaled mean-square end-to-end distance of bottlebrushes, $\langle R_0^2 \rangle / N_{bb}^{6/5}$, are plotted as a function of the scaling variable, $(1 + N_{sc}z)^{4/5}$. Our numerical

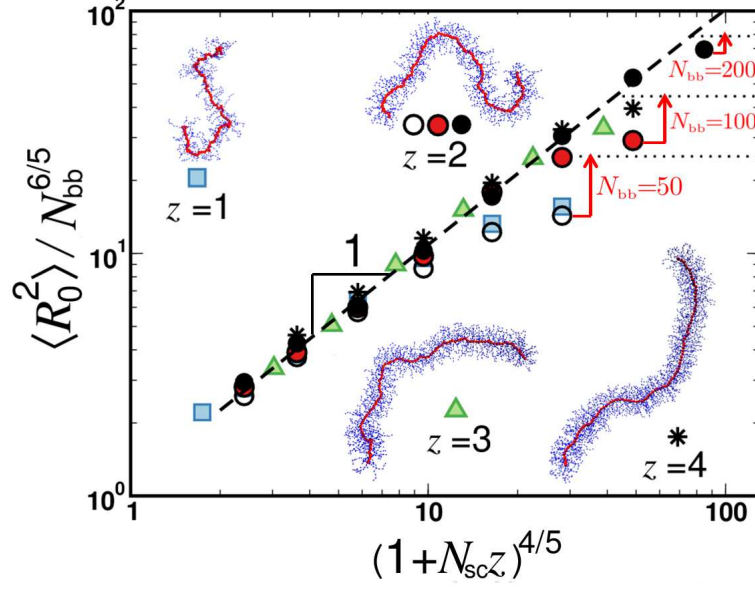


FIG. 3: Size of bottlebrushes in dilute solution. Mean-square end-to-end distance, $\langle R_0^2 \rangle$, of bottlebrushes in dilute solution (concentration $c = 10^{-3}$), normalized by the dependence of $\langle R_0^2 \rangle$ on the backbone's degree of polymerization in good solvent, $N_{bb}^{6/5}$, as a function of the scaling variable, $(1 + N_{sc}z)^{4/5}$. The dashed line represents the theoretical scaling law [see Eq. (6)]. The number of side chains grafted per backbone monomer is $z = 1$ (squares), 2 (circles), 3 (triangles), and 4 (stars). The degree of polymerization of backbones is fixed to $N_{bb} = 100$, apart of the data for $z = 2$, where $N_{bb} = 50$ (empty circles), 100 (red circles), and 200 (black circles). For data with $z = 2$, red arrows indicate the maximum square end-to-end distance corresponding to the fully extended backbone (horizontal dotted lines). Snapshots display conformations of macromolecules with $N_{bb} = 100$ for various values of z , as denoted. For all data points, error bars are smaller than symbol size.

data corroborate the scaling prediction of Eq. (6). The extension of the bottlebrush backbone caused by the increase of N_{sc} and z is due to the enhancement of steric repulsion between densely grafted side chains. The data in Fig. 3 also indicate that the mean-square size levels off for bottlebrushes whose backbones are too short. This is attributed to the finite extensibility of the backbone, which becomes more relevant with increasing values of N_{sc} and *decreasing* values of z . At first glance, the latter observation seems counter-intuitive, because one may assume that stretching of the backbone becomes more pronounced as both the number of monomers per side chains and the grafting density increase. Our theoretical approach reflects that decreasing the grafting density leads to a stronger effect of finite extensibility. The backbone remains semi-flexible, if the persistence length is sufficiently smaller than the overall extension of the macromolecule, i.e.,

$R_0/l \gg 1$. With Eqs. (4) and (6), one obtains the condition $N_{bb} \gg \sqrt{N_{sc}/z}$, which is in qualitative accordance with our observation from Fig. 3. Note that the effect of finite extensibility diminishes as the concentration is increased. For bottlebrushes with $N_{bb} \geq 100$, it has been shown that finite extensibility can be neglected under melt conditions [47]. In what follows, we restrict our analysis to the case of bottlebrushes with $N_{bb} = 100$.

Concentration-dependence of bottlebrush solutions

To study the dependence of conformational properties of bottlebrushes on concentration we incorporate the model of a bottlebrush in dilute solution, developed in the previous section, and perform scaling analysis (for detailed calculations, see Methods section). We predict a sequence of four regimes upon increasing concentration, as depicted in Fig. 4. For concentrations c with $c_1 < c < c_2$, macromolecules start to overlap and the excluded volume interaction is screened on the length scale comparable to the extension of the backbone. The screening results in a change of conformation from a self-avoiding walk of persistent segments into a random walk of these segments. This regime is similar to that for linear chains (without side chains), and the concentration dependence is the same, i.e., the mean-square end-to-end distance of the macromolecule scales as $R_1^2 \propto c^{-1/4}$ [79]. For larger concentrations, $c_2 < c < c_3$, the screening of excluded volume takes

x	c_x	Eq.	R_x^2	Eq.
0	—	—	$N_{bb}^{6/5} (N_{sc} z)^{4/5} c^0$	(6)
1	$N_{bb}^{-4/5} (N_{sc} z)^{-1/5}$	(15)	$N_{bb} (N_{sc} z)^{3/4} c^{-1/4}$	(17)
2	$N_{sc}^{-3/5} z^{1/5}$	(18)	$N_{bb} (N_{sc} z)^{4/5} c^{-1/2}$	(23)
3	$N_{sc}^{-13/20} z^{11/20}$	(24)	$N_{bb} N_{sc}^{1/2} z^{33/26} c^{-8/13}$	(28)
4	$N_{sc}^{-1/2} z^{7/26}$	(29)	$N_{bb} N_{sc}^{1/2} z^{157/130} c^{-4/5}$	(32)

TABLE I: Summary of the theoretically predicted overlap concentrations, c_x ($x = 0, \dots, 4$), and the corresponding mean-square end-to-end distances, R_x^2 , of bottlebrush macromolecules as functions of the degrees of polymerization of the backbone (N_{bb}) and the side chains (N_{sc}), grafting density of the side chains (z), and concentration (c).

place on a length scale comparable to the persistence length. As a consequence, the backbone monomers of the persistent segment now perform a random walk instead of self-avoiding walk

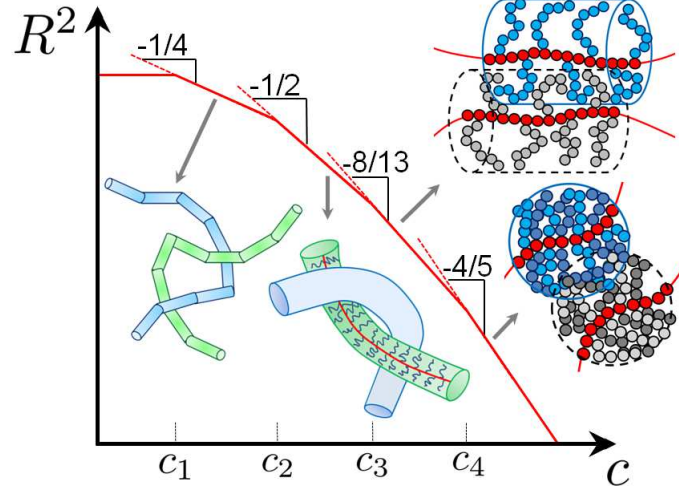


FIG. 4: **Hierarchical screening of excluded volume in solutions of bottlebrushes.** Dependence of mean-square end-to-end distance, R^2 , on concentration, c , for bottlebrush solutions, as predicted theoretically. Bottlebrushes undergo a hierarchical screening of excluded volume interactions at different length scales, which results in a sequence of decays in macromolecular size with characteristic exponents as indicated. The screening first takes place along the backbone of the macromolecule (regime 1 for $c_1 < c < c_2$), then along the persistence segment (regime 2 for $c_2 < c < c_3$), between side chains of different molecules (regime 3 for $c_3 < c < c_4$), and between side chains of the same molecule (regime 4 for $c > c_4$). The scaling predictions for the mean-square size of bottlebrushes in different concentration regimes and the corresponding overlap concentrations are listed in Table I. For detailed calculations, see Methods section.

[cf. Eq. (5)]. In this regime, we predict $R_2^2 \propto c^{-1/2}$. Once the concentration is increased even further, such that $c_3 < c < c_4$, side chains of different molecules start to screen each other, which yields a change of statistics for the side chains from self-avoiding walk to random walk. This leads to $R_3^2 \propto c^{-8/13}$. Finally, for highly concentrated solutions with $c > c_4$, the individual macromolecules are strongly compressed and intra-side chain screening occurs, where side chains of the same macromolecule can screen their excluded volume interaction. For this regime, we predict $R_4^2 \propto c^{-4/5}$. The different overlap concentrations and predictions for the macromolecular size of bottlebrushes in the corresponding regime of concentrations are summarized in Table I. Detailed calculations can be found in the Methods section.

The hierarchy of excluded volume screening is visualized by MD snapshots in Fig. 5. Here, we display bottlebrush conformations representing screening on different length scales for all theoretically derived concentration regimes ranging from semidilute to highly concentrated solutions.

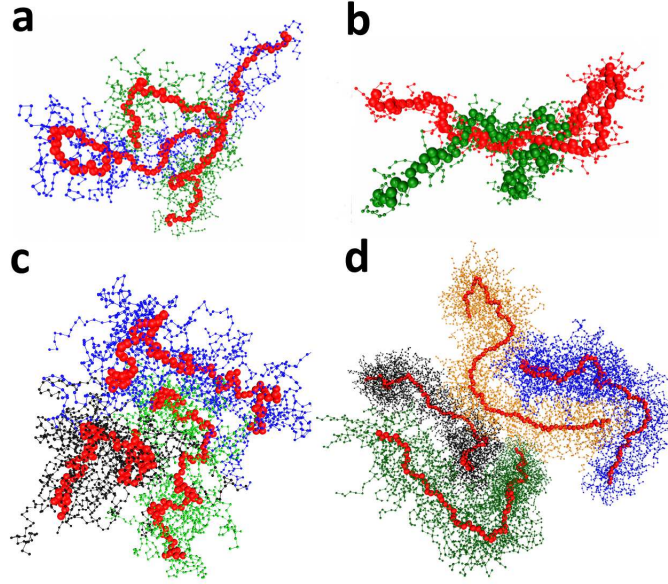


FIG. 5: Bottlebrush macromolecules in solutions at different concentrations. Simulation snapshots for bottlebrushes of different architecture displaying hierarchical screening of excluded volume interactions, which is observed at different regimes of concentration: **(a)** regime 1 ($c_1 < c < c_2$) – screening along the backbone ($N_{sc} = 8$, $z = 1$, $c = 0.2$), **(b)** regime 2 ($c_2 < c < c_3$) – screening along persistent segments ($N_{sc} = 4$, $z = 1$, $c = 0.7$), **(c)** regime 3 ($c_3 < c < c_4$) – intermolecular screening of the side chains ($N_{sc} = 32$, $z = 1/3$, $c = 0.8$), **(d)** regime 4 ($c > c_4$) – inter- and intra-molecular screening of the side chains ($N_{sc} = 16$, $z = 2$, $c = 0.8$). All macromolecules have the same degree of polymerization of the backbone, $N_{bb} = 100$, but different degrees of polymerization of the side chains, N_{sc} , and grafting density, z , as indicated in the parenthesis above.

Our simulations confirm the scaling predictions for the concentration-dependent size of bottlebrushes. The mean-square end-to-end distance, $\langle R^2(c) \rangle$, at concentration c for macromolecules of different architectures is plotted as a function of c in Fig. 6. The concentration regime 1 (cf. Fig. 5a), with scaling $R_1^2 \propto c^{-1/4}$ (dotted line), is observed independently of the degree of polymerization of side chains and grafting density. In particular, linear chains ($z = 0$) obey the well-known scaling result in the whole range of considered concentrations with $c > c_1$. The dependence of size on concentration for crew-cut bottlebrushes with $N_{sc} \lesssim 4$ (cf. Fig. 5b) is well described by the scaling law $R_2^2 \propto c^{-1/2}$ in regime 2 (dashed line). This is attributed to negligible screening of excluded volume interactions among side chain monomers. Consequently, macromolecules with short side chains remain in regime 2 for all concentrations with $c > c_2$. The regimes 3 and 4 incorporate screening of excluded volume by mutual side chain interactions and

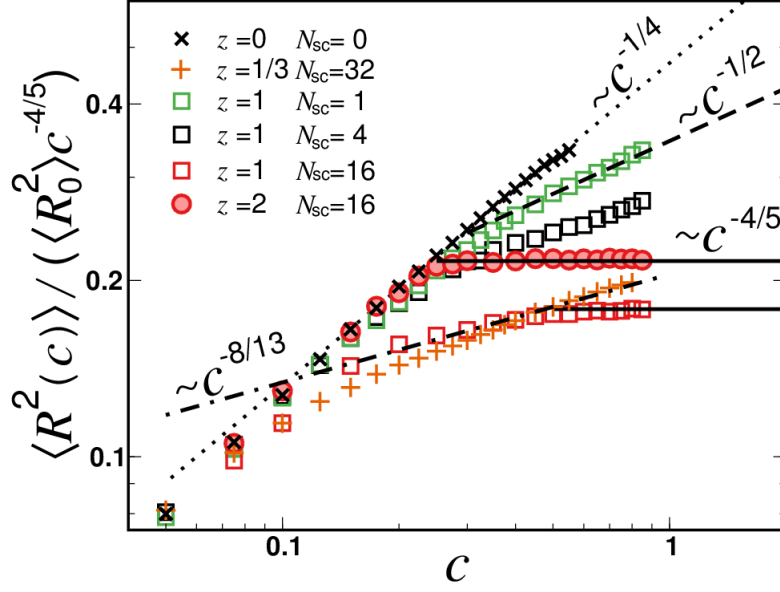


FIG. 6: **Concentration-dependent size of bottlebrushes.** Mean-square end-to-end distance, $\langle R^2(c) \rangle$, of bottlebrushes at concentration c normalized by their values at dilute concentration, $\langle R_0^2 \rangle$, and the theoretical scaling with concentration in a melt (regime 4), $c^{-4/5}$, as a function of c .

Lines represent theoretical scaling laws for the mean-square size of macromolecules in the corresponding regime of concentration: (dotted) regime 1 with $R_1^2 \propto c^{-1/4}$, (dashed) regime 2 with $R_2^2 \propto c^{-1/2}$, (dotted-dashed) regime 3 with $R_3^2 \propto c^{-8/13}$, and (solid) regime 4 with $R_4^2 \propto c^{-4/5}$. Data are shown for macromolecules with various degrees of polymerization of side chains, N_{sc} , and grafting densities of side chains, z , as indicated in the legend. The degree of polymerization of the backbone is fixed to $N_{bb} = 100$ for all data.

are relevant for macromolecules with long side chains ($N_{sc} \gtrsim 16$). For comb-like macromolecules with grafting density $z = 1/3$ (cf. Fig. 5c), inter-side chain screening occurs and the data reproduce the scaling in regime 3, $R_3^2 \propto c^{-8/13}$ (dotted-dashed line), for concentrated solutions with $c > c_3$. For bottlebrushes with $z = 1$ and $z = 2$ in melts (cf. Fig. 5d), the overlap between side chains of neighboring molecules is limited [47]. Thus, intra-side chain contacts dominate and are responsible for screening of excluded volume interactions. The latter conclusion corroborates with the numerical data, which display the scaling law $R_4^2 \propto c^{-4/5}$ of regime 4 (solid lines) for concentrations with $c > c_4$.

The structural properties of highly grafted bottlebrushes in melts, described by regime 4, are of fundamental importance in shaping mechanical and physical properties of novel polymeric materials. To perform a universal scaling plot for this regime, we derive [see Methods section,

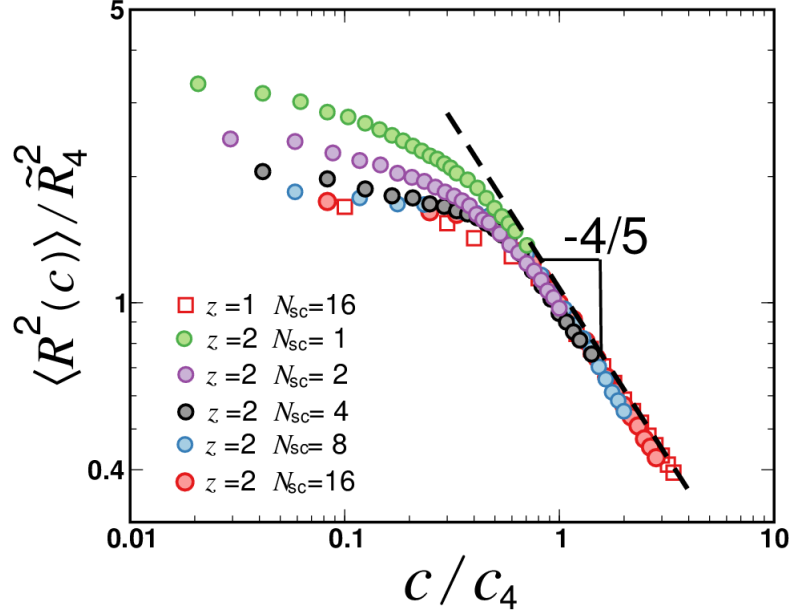


FIG. 7: Universal scaling plot of concentration-dependent size of bottlebrushes. Double-logarithmic scaling plot for bottlebrush extension versus concentration. The mean-square end-to-end distance, $\langle R^2(c) \rangle$, of bottlebrushes at concentration c is normalized by its value, $\tilde{R}_4^2 \propto N_{bb} N_{sc}^{9/10} z^{129/130}$, at the overlap concentration c_4 for regime 4 (melt) as a function of c normalized by $c_4 \propto N_{sc}^{-1/2} z^{7/26}$. The dashed line represents the theoretical scaling law for regime 4 (see Eq. 7). Data are for macromolecules with various degrees of polymerization of side chains, N_{sc} , and grafting densities of side chains, z , as indicated in the legend. The degree of polymerization of the backbone is fixed to $N_{bb} = 100$ for all data.

Eq. (32)]

$$\left(\frac{R_4^2}{\tilde{R}_4^2} \right) \propto \left(\frac{c}{c_4} \right)^{-4/5}, \quad (7)$$

with $\tilde{R}_4^2 \propto N_{bb} N_{sc}^{9/10} z^{129/130}$ and $c_4 \propto N_{sc}^{-1/2} z^{7/26}$. We test the prediction of Eq. (7) in Fig. 7 and find a striking agreement with the data from the MD simulations. Figure 7 demonstrates that the universal scaling plot enables superposition of all data onto a master curve for concentrations with $c > c_4$. We emphasize that we have not introduced any numerical pre-factors. This means that the proportionality sign in Eq. (7) can be replaced by an equality sign and all pre-factors cancel out. The scaling plot should be particularly useful for experimental data, which may become available in the near future.

In theory, scaling plots like the one displayed in Fig. 7 can be constructed for all concentration regimes. However, one needs a clear separation of the involved length scales, such that the different concentration regimes are wide enough. The width of an individual concentration regime follows

from the ratio of consecutive overlap concentrations, see Table I. In simulations, the separation of length scales is very difficult to achieve, because one needs bottlebrushes with relatively large backbones and side chains, which requires significant computational efforts.

Discussion

The hierarchical screening of excluded volume interactions in bottlebrush solutions stems from a variety of length scales characterizing their architecture and leads to distinct scaling regimes for their conformational properties. We demonstrated that the behavior of the concentration-dependent size known for linear chains (without grafted side chains) is reproduced as long as the size of the backbone represents the only relevant length scale. This condition is fulfilled for low concentrations just above the onset of macromolecular overlap. As the concentration is increased, screening emerges on the substructure of the macromolecule. First, the persistence length, the length at which the backbone monomers are correlated due to steric repulsion of the grafted side chains, becomes the next lower relevant length scale. Upon further increase of the concentration, the length of grafted side chains comes into play. Here, we observe the consequences of excluded volume screening along the interacting side chains of different macromolecules. For melts of bottlebrushes with sufficiently long side chains, an ultimate regime appears due to screening of excluded volume among side chains within the same macromolecule.

Our theoretical approach differs from the previous model by Borisov *et al.* [37], but we obtain a very similar scaling law in the regime of concentrated solutions (regime 3), where inter-side chain screening dominates conformational properties. However, the concentration regime that is characterized by intra-molecular side chain screening (regime 4) has not been anticipated before. Our MD simulation provides a significant and successful verification of this novel regime. The available results from scattering experiments [54] indicate a decrease in bottlebrush size with increasing concentration, but an accurate comparison to scaling predictions is not possible yet, due to the limited number of data points. Therefore, we believe that our results will stimulate new experimental investigations.

Our study demonstrates that conformations of branched macromolecules display hierarchical transitions facilitated by screening of excluded volume interactions on various length scales. This phenomenon is generic in nature and does not depend on the specific arrangement of grafting nodes. A broad range of polymeric architectures, including dendromers, dendronized, pom-pom-shaped and star-burst polymers, are expected to demonstrate similar hierarchical screening effects. Therefore, our work presents valuable insights into structural properties of topologically complex polymers in solutions and melts.

Materials and Methods

Molecular dynamics simulations

Simulations of bottlebrush, comb-like, and linear polymer solutions are performed using the coarse-grained bead-spring model of Kremer and Grest [80]. An individual macromolecule is composed of N_{bb} backbone monomers (modeled as excluded volume spheres), which are connected by bonds. To these backbone monomers, we connect side chains with grafting density z . Each side chain contains N_{sc} monomers, which are identical to the monomers of the backbone. The total number of beads in a molecule is $N_{\text{bb}}(1 + N_{\text{sc}}z)$.

The non-bonded interactions between monomers separated by a distance r are modeled by the truncated and shifted Lennard-Jones (LJ) potential,

$$V^{\text{LJ}}(r) = \begin{cases} 4\epsilon [(\sigma/r)^{12} - (\sigma/r)^6 + C] & r \leq r_c \\ 0 & r > r_c, \end{cases} \quad (8)$$

where the interaction strength, ϵ , is measured in units of thermal energy, $k_{\text{B}}T$, σ is the monomer diameter, r_c is the cutoff, and C is the shift of the potential introduced to avoid a discontinuity at $r = r_c$. We use $\epsilon = k_{\text{B}}T$, $C = 1/4$, and $r_c = 2^{1/6} \sigma$. This choice of parameters results in purely repulsive interactions between monomers, ensuring good solvent conditions at all values of $k_{\text{B}}T$.

The bonded interactions in a molecule are mimicked by the Kremer-Grest potential [80], $V^{\text{KG}}(r) = V^{\text{FENE}}(r) + V^{\text{LJ}}(r)$, with the “finitely extensible nonlinear elastic” (FENE) potential

$$V^{\text{FENE}} = -\frac{1}{2}kr_{\text{F}}^2 \ln \left[1 - \left(\frac{r}{r_{\text{F}}} \right)^2 \right]. \quad (9)$$

Here, the bond spring-constant is $k = 30 \epsilon/\sigma^2$, and the maximum bond length is $r_{\text{F}} = 1.5 \sigma$ [80]. All simulations are performed in a cubic box with periodic boundary conditions imposed in all spatial dimensions.

We use the Velocity-Verlet algorithm [81] to solve the Langevin equation of motion for the position \mathbf{r}_i of each monomer with mass m ,

$$m\ddot{\mathbf{r}}_i = \mathbf{F}_i^{\text{LJ}} + \mathbf{F}_i^{\text{FENE}} - \zeta\dot{\mathbf{r}}_i + \mathbf{F}_i^{\text{R}}. \quad (10)$$

The forces \mathbf{F}_i^{LJ} and $\mathbf{F}_i^{\text{FENE}}$ respectively follow from the LJ (Eq. 8) and the FENE (Eq. 9) interaction potentials. The third and fourth term on the right hand side of Eq. (10) are a slowly evolving viscous force, $-\zeta\dot{\mathbf{r}}_i$, and a rapidly fluctuating stochastic force, \mathbf{F}_i^{R} . The random force, \mathbf{F}_i^{R} , is related to the friction coefficient, ζ , by the fluctuation-dissipation theorem, $\langle \mathbf{F}_i^{\text{R}}(t) \mathbf{F}_j^{\text{R}}(t') \rangle = k_{\text{B}}T\zeta\delta_{ij}\delta(t-t')$. The friction coefficient used in our simulations is $\zeta = 0.5 m\tau^{-1}$, where $\tau = \sqrt{m\sigma^2/\epsilon}$ is the LJ time unit. The integration step is taken to be $\Delta\tau = 0.005\tau$, and the thermal energy is constant at $k_{\text{B}}T = 1$. All simulations are carried out using the Large-scale Atomic/Molecular Massively Parallel Simulator (LAMMPS) [82], and the simulation snapshots are rendered using the program Visual Molecular Dynamics (VMD) [83]. Initially, molecules are grown using a self-avoiding random walk technique and placed randomly in the simulation cell. The initial concentration of all systems is small, $c \approx 5 \cdot 10^{-4} \sigma^{-3}$. To obtain the desired concentration, the simulation box is gradually decreased in size at constant velocity $10^{-3} \sigma/\tau$. Once the target density is reached, simulations are continued for up to at least three relaxation times of the corresponding system. During the equilibration stage, the molecules diffuse on average at least over the root-mean-square end-to-end distance of their backbones.

Simulations of solutions are carried out for linear ($z = 0$), comb-like ($z = 1/3$), and bottle-brush ($z \geq 1$) polymers for a fixed number of backbone monomers, $N_{\text{bb}} = 100$, in the range of concentration varied from $c = 0.001 \sigma^{-3}$ (dilute solutions) to $c = 0.85 \sigma^{-3}$ (melts). The number

of monomers per side chain is varied between $N_{\text{sc}} = 0$ and $N_{\text{sc}} = 16$ for bottlebrushes with $z = 1$ or $z = 2$ side chains attached to each backbone monomer. For macromolecules with $z = 1/3$, the number of side chains monomers is fixed to $N_{\text{sc}} = 32$. In addition, for dilute solutions of bottlebrushes ($c = 0.001 \sigma^{-3}$), the number of backbone monomers is varied ($N_{\text{bb}}=50, 100$, and 200) as well as the number of side chain monomers ($N_{\text{sc}} = 1, 2, 4, 8, 16, 32$, and 64) and the grafting density ($z = 1, 2, 3$, and 4).

Scaling analysis

Before presenting our scaling analysis for the concentration-dependent properties of bottlebrush conformations, we would like to discuss briefly how our approach compares to the previous models by Birshstein *et al.* [36] and Fredrickson [39], which start out from rod-like backbones, at least, on a local scale. To do so, we revisit our starting point, the free energy of the cylindrical subsegment as given by Eq. (1). Instead of minimizing the free energy with respect to l_0 and $R_{\text{sc},0}$, one may assume a stiff backbone inside the cylinder, i.e., $l_0 \propto n_0$. Minimization of F with respect to $R_{\text{sc},0}$ then yields

$$R_{\text{sc},0} \propto N_{\text{sc}}^{3/4} z^{1/4}. \quad (11)$$

The above scaling law for the size of side chains is known for bottlebrushes with rod-like backbones, see Refs. [36, 39, 84].

The spatial distance between grafting points for bottlebrushes with rod-like backbones, d , may be derived from a simple scaling approach,

$$R_{\text{sc},0} = \tilde{g}(r_0/d) \propto N_{\text{sc}}^{3/4} z^{1/4}, \quad (12)$$

where $r_0 \propto N^{3/5}$ denotes the size of a linear (not grafted) chain in dilute solution, and $\tilde{g}(x)$ is a scaling function. This ansatz leads to

$$d \propto z^{-1} \quad (13)$$

and, thus, to a rigid backbone inside the cylinder. The very same idea can be applied to the side

chain scaling derived in the main text for bottlebrushes with semi-flexible backbones [see Eq. (3) in the limit $N_{\text{sc}}z \gg 1$, i.e., $R_{\text{sc}} \propto N_{\text{sc}}^{7/10} z^{1/10}$]. The scaling argument yields

$$d \propto z^{-3/5}, \quad (14)$$

such that the spatial distance between grafting points resembles a self-avoiding walk statistics [79]. This is the fundamental difference between the scaling law of Eq. (11) and our result, cf. Eq. (3).

In the following, we present our scaling analysis for concentrations ranging from semi-dilute solutions to melts. The macromolecules start to overlap as the concentration is increased above their overlap concentration, $c > c_1$. With Eq. (6), the overlap concentration reads

$$c_1 \propto \frac{N_{\text{bb}}(1 + N_{\text{sc}}z)}{R_0^3} \propto N_{\text{bb}}^{-4/5} (1 + N_{\text{sc}}z)^{-1/5}. \quad (15)$$

In the semi-dilute regime, the screening of excluded volume interactions along the backbones is due to the presence of other macromolecules and leads to a random walk of the persistence segments [79]. Therefore, the size of a bottlebrush scales with the number of backbone monomers as

$$R_1 \propto R_0 \tilde{g}_1(c/c_1) \propto N_{\text{bb}}^{1/2}, \quad (16)$$

where $\tilde{g}_1(x)$ is a scaling function. Together with Eqs. (6) and (15), we obtain the size of a bottlebrush in concentration regime 1, which reads

$$R_1 \propto (1 + N_{\text{sc}}z)^{3/8} N_{\text{bb}}^{1/2} c^{-1/8}. \quad (17)$$

Note that for macromolecules with $N_{\text{sc}}z = 0$, Eq. (17) reproduces the expected power law dependence for linear chains, $R_{\text{linear}} \propto N_{\text{bb}}^{1/2} c^{-1/8}$ [79], which has been confirmed experimentally [85] and by computer simulations [86, 87].

Upon further increase of concentration, $c > c_2$, the persistence segments of neighboring bottle-

brushes start to overlap. The corresponding overlap concentration reads

$$c_2 \propto \frac{n_0(1 + N_{\text{sc}}z)}{l_0 R_{\text{sc},0}^2} \propto \left(\frac{N_{\text{sc}}}{z}\right)^{-2/5} (1 + N_{\text{sc}}z)^{-1/5}, \quad (18)$$

where we have used Eqs. (4) and (5). In concentration regime 2, the self-avoiding walk of monomers inside the cylinder turns into a random walk. Since the excluded volume contribution of the side chains remains unaltered, one may anticipate that the persistence length in this regime is given by

$$l_2 \propto n_2^{1/2} (1 + N_{\text{sc}}z)^{2/5}. \quad (19)$$

A priori, we do not know how the number of backbone monomers inside the cylinder for regime 2, n_2 , depends on N_{sc} and z . However, we may assume that n_2 remains proportional to $z^{-1/2}$, see Eq. (4). Thus, in the limit $N_{\text{sc}}z \gg 1$, Eq. (19) suggests $l_2 \propto z^{3/20}$. The latter result allows us to perform a crossover scaling,

$$l_2 \propto l_0 \tilde{g}_2(c/c_2) \propto z^{3/20}, \quad (20)$$

with $\tilde{g}_2(x)$ a scaling function. Together with Eq. (5) and $N_{\text{sc}}z \gg 1$, Eq. (20) leads to

$$l_2 \propto R_{\text{sc},2} \propto N_{\text{sc}}^{11/20} z^{3/20} c^{-1/4}, \quad (21)$$

where $R_{\text{sc},2}$ denotes the size of side chains in regime 2. Within our theoretical picture, both persistence length and size of side chains depend on concentration, but the number of backbone monomers per cylindrical segment in a given concentration regime does not. Thus, Eq. (21) suggests a decreasing persistence (side chain) length with a constant number of backbone monomers inside the persistence segment.

Equation (21) can be re-written as $l_2 \propto N_{\text{sc}}^{3/20} z^{-1/4} (N_{\text{sc}}z)^{2/5} c^{-1/4}$. Together with Eq. (19) and $N_{\text{sc}}z \gg 1$, we obtain

$$n_2 \propto \sqrt{\frac{N_{\text{sc}}^{3/5}}{z}}, \quad (22)$$

which reflects a natural modification of Eq. (4). With Eqs. (21) and (22), we obtain the macro-

molecular size of bottlebrushes in regime 2 ($N_{\text{sc}}z \gg 1$),

$$R_2 \propto (1 + N_{\text{sc}}z)^{2/5} N_{\text{bb}}^{1/2} c^{-1/4}. \quad (23)$$

Once the concentration is increased even further, $c > c_3$, the macromolecules attain melt concentration and side chains of neighboring macromolecules start to overlap. The corresponding overlap concentration reads

$$c_3 \propto \frac{N_{\text{sc}}z}{l_2 R_{\text{sc},2}^2} \propto N_{\text{sc}}^{-13/20} z^{11/20}, \quad (24)$$

where Eq. (21) in the limit $N_{\text{sc}}z \gg 1$ has been used. Due to the screening of excluded volume interactions along the side chains of neighboring macromolecules, one expects that the size of side chains, $R_{\text{sc},3}$, and the corresponding persistence length, l_3 , in regime 3 scale as $R_{\text{sc},3} \propto l_3 \propto N_{\text{sc}}^{1/2}$. With $\tilde{g}_3(x)$ a scaling function, the crossover scaling

$$l_3 \propto l_0 \tilde{g}_3(c/c_3) \propto N_{\text{sc}}^{1/2} \quad (25)$$

leads to

$$l_3 \propto R_{\text{sc},3} \propto N_{\text{sc}}^{1/2} z^{7/26} c^{-4/13}, \quad (26)$$

where we have used Eqs. (5) and (24) in the limit $N_{\text{sc}}z \gg 1$. In highly concentrated solutions, the persistence length is proportional to the number of side chains within the cylinder, i.e., $l_3 \propto n_3 z$.

With Eq. (26), the number of backbone monomers in the cylinder then is

$$n_3 \propto N_{\text{sc}}^{1/2} z^{-19/26}. \quad (27)$$

The size of bottlebrushes in regime 3, R_3 , follows from a random walk of persistence segments with length l_3 , where each segment contains n_3 backbone monomers. This yields

$$R_3 \propto l_3 \left(\frac{N_{\text{bb}}}{n_3} \right)^{1/2} \propto N_{\text{bb}}^{1/2} N_{\text{sc}}^{1/4} z^{33/52} c^{-4/13}. \quad (28)$$

The above scaling result is very close to the one predicted by Borisov *et al.* [37] with respect to all

four exponents. However, the underlying assumptions for both models are different. The scaling of bottlebrush size with N_{bb} and N_{sc} has been confirmed recently under melt conditions [47].

With respect to suppressing entanglement effects in order to design super-elastic rubbers, highly grafted bottlebrushes are of particular interest. Here, an additional regime can appear, where compression of the backbone and the side chains can lead to mutual screening of side chains that belong to the same macromolecule. With Eq. (26), the overlap concentration in regime 4 is

$$c_4 \propto \frac{N_{\text{sc}} z}{R_{\text{sc},3}^3} \propto N_{\text{sc}}^{-1/2} z^{7/26}. \quad (29)$$

The crossover scaling reads

$$l_4 \propto l_0 \tilde{g}_4(c/c_4) \propto N_{\text{sc}}^{1/2}, \quad (30)$$

with $\tilde{g}_4(x)$ a scaling function. Using Eq. (5) in the limit $N_{\text{sc}} z \gg 1$, one obtains the concentration dependence of the persistence length in regime 4,

$$l_4 \propto N_{\text{sc}}^{1/2} z^{27/130} c^{-2/5}. \quad (31)$$

Once more, we assume local stretching of the backbone, i.e., $l_4 \propto n_4 z$, where n_4 denotes the number of backbone monomers per persistent segment for regime 4. With Eq. (31), this leads to

$$R_4 \propto l_4 \left(\frac{N_{\text{bb}}}{n_4} \right)^{1/2} \propto N_{\text{bb}}^{1/2} N_{\text{sc}}^{1/4} z^{157/260} c^{-2/5}, \quad (32)$$

for the size of bottlebrushes in regime 4. Together with Eq. (29), the above equation can be rewritten, such that we obtain Eq. (7) of the main text.

Acknowledgments:

The authors thank A. Johner and J.-U. Sommer for fruitful discussions. J.P. thanks for computational time at PL-Grid (Poland) and ZIH (Germany) infrastructures.

Funding:

J.P. acknowledges support from the German Science Foundation (DFG-Pa 2860/2-1) and the Polish Ministry of Science and Higher Education (IP 2015 059074). T.K. thanks the German Science Foundation (DFG-Kr 2854-2) for financial support.

-
- [1] Sheiko, S. S. Sumerlin, B. S. & Matyjaszewski, K. Cylindrical molecular brushes: Synthesis, characterization, and properties. *Prog. Polym. Sci.* **33**, 759 (2008).
- [2] Rzaev, J. Molecular bottlebrushes: New opportunities in nanomaterials fabrication. *ACS Macro Lett.* **1**, 1146 (2012).
- [3] Verduzco, R. Li, X. Pesek, S. L. & Stein, G. E. Structure, function, self-assembly, and applications of bottlebrush copolymers. *Chem. Soc. Rev.* **44**, 2405 (2015).
- [4] Müllner, M. & Müller, A. H. E. Cylindrical polymer brushes - Anisotropic building blocks, unimolecular templates and particulate nanocarriers. *Polymer* **98**, 389 (2016).
- [5] Beers, K. L. *et al.* The synthesis of densely grafted copolymers by atom transfer radical polymerization. *Macromolecules* **31**, 9413 (1998).
- [6] Li, Z. *et al.* Facile syntheses of cylindrical molecular brushes by a sequential RAFT and ROMP grafting-through methodology. *J. Polym. Sci. Part A: Polym. Chem.* **47**, 5557 (2009).
- [7] Jha, S. Dutta, S. & Bowden, N. B. Synthesis of ultralarge molecular weight bottlebrush polymers using Grubbs' catalysts. *Macromolecules* **37**, 4365 (2004).
- [8] Xia, Y. Kornfield, J. A. & Grubbs, R. H. Efficient synthesis of narrowly dispersed brush copolymers and study of their assemblies: The importance of side chain arrangement. *Macromolecules* **42**, 3761 (2009).
- [9] Zhang, M. & Möller, A. H. Cylindrical polymer brushes. *J. Polym. Sci., Part A: Polym. Chem.* **43**, 3461 (2005).
- [10] Ohno, S. & Matyjaszewski, K. Controlling grafting density and side chain length in poly(n-butyl acrylate) by ATRP copolymerization of macromonomers. *J. Polym. Sci., Part A: Polym. Chem.* **44**, 5454 (2006).
- [11] Matsuda, M. Satoh, K. & Kamigaito, M. Periodically functionalized and grafted copolymers via 1:2-sequence-regulated radical copolymerization of naturally occurring functional limonene and maleimide derivatives. *Macromolecules* **46**, 5473 (2013).
- [12] Bielawski, C. W. & Grubbs, R. H. Living ring-opening metathesis polymerization. *Prog. Polym. Sci.* **32**, 1 (2007).
- [13] Lin, T.-Z. *et al.* Control of grafting density and distribution in graft polymers by living ring-opening metathesis copolymerization. *J. Am. Chem. Soc.* **139**, 3896 (2017).
- [14] Wintermantel, M. *et al.* Rodlike combs. *Macromol. Rapid Commun.* **15**, 279 (1994).
- [15] Pakula, T. *et al.* Molecular brushes as super-soft elastomers. *Polymer* **47**, 7198 (2006).
- [16] Daniel, W. F. M. *et al.* Solvent-free, supersoft and superelastic bottlebrush melts and networks. *Nature Mat.* **15**, 183 (2016).
- [17] Johnson, J. A. *et al.* Core-clickable PEG-branch-azide bivalent-bottle-brush polymers by ROMP: Grafting-through and clicking-to. *J. Am. Chem. Soc.* **133**, 559 (2010).
- [18] Xu, H. *et al.* Molecular Pressure Sensors. *Adv. Mater.* **19**, 2930 (2007).
- [19] Li, X. Prukop, S. L. Biswal, S. L. & Verduzco, R. Surface properties of bottlebrush polymer thin films. *Macromolecules* **45**, 7118 (2012).
- [20] Peng, S. & Bhushan, B. Smart polymer brushes and their emerging applications. *RSC Advances* **2**, 8557 (2012).
- [21] Zhang, Q. *et al.* RAFT polymerization to form stimuli-responsive polymers. *J. Colloid Polym. Sci.* **294**, 1705 (2016).

- [22] Faivre, J. *et al.* Wear protection without surface modification using a synergistic mixture of molecular brushes and linear polymers. *et al. ACS Nano* **11**, 1762 (2017).
- [23] Xie, G. Krys, P. Tilton, R. T. & Matyjaszewski, K. Heterografted molecular brushes as stabilizers for water-in-oil emulsions. *Macromolecules* (2017) DOI: 10.1021/acs.macromol.7b00006
- [24] Banquy, X. *et al.* Bioinspired bottle-brush polymer exhibits low friction and amontons-like behavior. *J. Am. Chem. Soc* **136**, 6199 (2014).
- [25] Bolton, J. Bailey, T. S. & Rzaev, J. Large pore size nanoporous materials from the self-assembly of asymmetric bottlebrush block copolymers. *Nano Lett.* **11**, 998 (2011).
- [26] Runge, M. B. & Bowden, N. B. Synthesis of high molecular weight comb block copolymers and their assembly into ordered morphologies in the solid state. *J. Am. Chem. Soc.* **129**, 10551 (2007).
- [27] Noel, A. Borguet, Y. P. & Wooley, K. L. Self-reporting degradable fluorescent grafted copolymer micelles derived from biorenewable resources. *ACS Macro Letters* **4**, 645 (2015).
- [28] Zhang, J. *et al.* Design of graft block polymer thermoplastics. *Macromolecules* **49**, 9108 (2016).
- [29] Sun, G. *et al.* Nanoscopic cylindrical dual concentric and lengthwise block brush terpolymers as covalent preassembled high-resolution and high-sensitivity negative-tone photoresist materials. *J. Am. Chem. Soc.* **135**, 4203 (2013).
- [30] Bates, C. M. *et al.* Brush polymer ion gels. *J. Polym. Sci. Part B: Polym. Phys.* **54**, 292 (2016).
- [31] Sveinbjörnsson, B. R. *et al.* Rapid self-assembly of brush block copolymers to photonic crystals. *Proc. Natl. Acad. Sci.* **109**, 14332 (2012).
- [32] Bates, C. M. *et al.* ABA triblock brush polymers: synthesis, self-assembly, conductivity, and rheological properties. *Macromolecules* **48**, 4967 (2015).
- [33] Button, B. *et al.* Periciliary brush promotes the lung health by separating the mucus layer from airway epithelia. *Science* **337**, 937 (2012).
- [34] Khalsa, P. S. & Eisenberg, S. R. Compressive behavior of articular cartilage is not completely explained by proteoglycan osmotic pressure. *J. Biomech.* **30**, 589 (1997).
- [35] Scott, J. E. Proteodermatan and proteokeratan sulfate (decorin, lumican/fibromodulin) proteins are horseshoe shaped. Implications for their interactions with collagen. *Biochemistry* **35**, 8795 (1996).
- [36] Birshtein, T. M. *et al.* Conformations of comb-like macromolecules. *Polym. Sci. U.S.S.R.* **29**, 1293 (1987).
- [37] Borisov, O. V. Birshtein, T. M. & Zhulina, Y. B. The temperature-concentration diagram of state for solutions of comb-like macromolecules. *Polym. Sci. U.S.S.R.* 1987, **29**, 1552.
- [38] Rouault, Y. & Borisov, O. V. Comb-branched polymers: Monte Carlo simulation and scaling. *Macromolecules* **29**, 2605 (1996).
- [39] Fredrickson, G. H. Surfactant-induced lyotropic behavior of flexible polymer solutions. *Macromolecules* **26**, 2825 (1993).
- [40] Denesyuk, N. A. Conformational properties of bottle-brush polymers. *Phys. Rev. E* **67**, 051803 (2003).
- [41] Potemkin, I. I. Persistence length of comblike polymers strongly adsorbed on a flat surface. *Macromolecules* **39**, 7178 (2006).
- [42] Wang, Y. *et al.* Mean span dimensions of ideal polymer chains containing branches and rings. *Macromolecules* **44**, 403 (2011).
- [43] Subbotin, A. Saariaho, M. Ikkala, O. & ten Brinke, G. Elasticity of comb copolymer cylindrical brushes. *Macromolecules* **33**, 3447 (2000).
- [44] Nakamura, Y. & Norisuye, T. Backbone stiffness of comb-branched polymers. *Polym. J.* **33**, 874 (2001).
- [45] Conolly, R. *et al.* "Intrinsic" and "topological" stiffness in branched polymers. *Macromolecules* **38**, 5288 (2005).

- [46] Feuz, L. Leermakers, F. A. M. Textor, M. & Borisov, O. Bending rigidity and induced persistence length of molecular bottle brushes: A self-consistent-field theory. *Macromolecules* **38**, 8891 (2005).
- [47] Paturej, J. Sheiko, S. S. Panyukov, S. & Rubinstein, M. Molecular structure of bottlebrush polymers in melts. *Sci. Adv.* **2**, e1601478 (2016).
- [48] Cao, Z. *et al.* Dynamics of bottlebrush networks. *Macromolecules* **49**, 8009 (2016).
- [49] Wintermantel, M. *et al.* Molecular bottlebrushes. *Macromolecules* **29**, 978 (1996).
- [50] Lecommandoux, S. *et al.* Effect of dense grafting on the backbone conformation of bottlebrush polymers: Determination of the persistence length in solution. *Macromolecules* **35**, 8878 (2002).
- [51] Rathgeber, S. *et al.* On the shape of bottle-brush macromolecules: Systematic variation of architectural parameters. *J. Chem. Phys.* **122**, 124904 (2005).
- [52] Vlassopoulos, D. *et al.* Polymacromonomers: structure and dynamics in nondilute solutions, melts, and mixtures *Macromolecules* **33**, 5960 (2000).
- [53] Pesek, S. L. *et al.* Small-angle neutron scattering analysis of bottlebrush polymers prepared via grafting-through polymerization. *Macromolecules* **46**, 6998 (2013).
- [54] Bolisetty, S. *et al.* Softening of the stiffness of bottle-brush polymers by mutual interaction. *Phys. Rev. E* **75**, 040803 (2007).
- [55] Feuz, L. *et al.* Conformation of poly(L-lysine)-graft-poly(ethylene glycol) molecular brushes in aqueous solution studied by small-angle neutron scattering. *Eur. Phys. Jour. E* **23**, 237 (2007).
- [56] Fisher, K & Schmidt M. Solvent-induced length variation of cylindrical brushes. *Macromol. Rapid Comm.* **22**, 787 (2001).
- [57] Zhang, B. *et al.* Conformation of cylindrical brushes in solution: effect of side chain length. *Macromolecules* **39**, 8440 (2006).
- [58] Cheng, G. *et al.* Small angle neutron scattering study of conformation of oligo(ethylene glycol)-grafted polystyrene in dilute solutions: effect of the backbone length. *Macromolecules* **41**, 9831 (2008).
- [59] Liu, W. *et al.* Coil-to-rod conformational transition and single chain structure of graft copolymer by tuning the graft density. *Polymer* **53**, 1005 (2012).
- [60] Zhang, Z. *et al.* Atomistic structure of bottlebrush polymers: Simulations and neutron scattering studies. *Macromolecules* **47**, 5808 (2014).
- [61] Kikuchi, M. *et al.* Graft density dependence of main chain stiffness in molecular rod brushes. *Macromolecules* **48**, 5878 (2015).
- [62] Iwawaki, H. Urakawa, O. Inoue T. & Nakamura Y. Rheo-optical study on dynamics of bottlebrush-like polymacromonomer consisting of polystyrene. II. Side chain length dependence on dynamical stiffness of main chain. *Macromolecules* **45**, 4801 (2012).
- [63] Tera, K. Hokajo, T. Nakamura Y. & Norisuye T. Solution properties of polymacromonomers consisting of polystyrene. 3. Viscosity behavior in cyclohexane and toluene. *Macromolecules* **32**, 3690 (1999).
- [64] Saariaho, M. *et al.* On lyotropic behavior of molecular bottle-brushes: A Monte Carlo computer simulation study. *J. Chem. Phys.* **107**, 3267 (1997).
- [65] Saariaho, M. Szleifer, I. Ikkala, M. & ten Brinke, G. Extended conformations of isolated molecular bottle-brushes: Influence of side-chain topology. *Macromol. Theory Simul.* **7**, 211 (1998).
- [66] Subbotin, A. Saariaho, Ikkala, M. & ten Brinke, G. Cylindrical brushes of comb copolymer molecules containing rigid side chains. *Macromolecules* **2000**, **33**, 3447.
- [67] Elli, S. *et al.* Size and persistence length of molecular bottle-brushes by Monte-Carlo simulations *J. Chem. Phys.* **120**, 6257 (2004).
- [68] Yethiraj, A. A. Monte-Carlo simulation study of branched polymers. *J. Chem. Phys.* **125**, 204901 (2006).
- [69] Hsu, H.-P. Paul, W. & Binder, K. Structure of bottle-brush polymers in solution: A Monte Carlo test

- of models for the scattering function *J. Chem. Phys.* **129**, 204904 (2008).
- [70] Hsu, H.-P. Paul, W. & Binder, K. Characteristic length scales and radial monomer density profiles of molecular bottle-brushes: simulation and experiment. *Macromolecules* **43**, 3094 (2010).
 - [71] Theodorakis, P. E. Hsu, H.-P. Paul, W. & Binder, K. Computer simulation of bottle-brush polymers with flexible backbone: Good solvent versus theta solvent conditions. *J. Chem. Phys.* **135**, 164903 (2011).
 - [72] Paturej, J. Kuban, Ł. Milchev, A. & Vilgis, T. A. Tension enhancement in branched macromolecules upon adhesion on a solid substrate. *EPL* **97**, 58003 (2012).
 - [73] Liang, H. *et al.* Combs and bottlebrushes in a melt. *Macromolecules* **50**, 3430 (2017).
 - [74] Milchev, A. Paturej, J. Rostiashvili, V. G. & Vilgis, T. A. Thermal degradation of adsorbed bottle-brush macromolecules: A molecular dynamics simulation. *Macromolecules* **44**, 3981 (2011).
 - [75] Neugebauer, D. *et al.* Densely-grafted and double-grafted PEO brushes via ATRP. A route to soft elastomers. *Macromolecules* **36**, 6746 (2003).
 - [76] Hu, M. *et al.* Linear rheological response of a series of densely branched brush polymers. *Macromolecules* **44**, 6935 (2011).
 - [77] Lopez-Barron, C. R. Brant, P. Eberle, A. P. & Crowther, D. J. Linear rheology and structure of molecular bottlebrushes with short side chains. *J. Rheol.* **59**, 865 (2015).
 - [78] Dalsin, S. J. Hillmyer, M. A. & Bates, F. S. Linear rheology of polyolefin-based bottlebrush polymers. *Macromolecules* **48**, 4680 (2015).
 - [79] de Gennes, P.-G. *Scaling concepts in polymer physics* (Cornell Univ. Press, NY, 1979).
 - [80] Kremer, K. & Grest, G. S. Dynamics of entangled linear polymer melts: A molecular-dynamics simulation. *J. Chem. Phys.* **92**, 5057 (1990).
 - [81] Verlet, L. Computer "experiments" on classical fluids. I. Thermodynamical properties of Lennard-Jones molecules. *Phys. Rev.* **159**, 98 (1967).
 - [82] Plimpton, S. J. Fast parallel algorithms for short-range molecular dynamics. *J. Comp. Phys.* **117**, 1 (1995) (<http://lammps.sandia.gov>).
 - [83] Humphrey, W. Dalke, A. & Schulten, K. VMD: Visual molecular dynamics. *J. Molec. Graphics* **14**, 33 (1996).
 - [84] Wang, Z.-G. & Safran, S. A. Size distribution for aggregates of associating polymers. II. Linear packing. *J. Chem. Phys.* **89**, 5323 (1988).
 - [85] Daoud, M. *et al.* Solutions of flexible polymers. Neutron experiments and interpretation. *Macromolecules* **8**, 804 (1975).
 - [86] Paul, W. Binder, K. Heermann, D. W. & Kremer, K. Crossover scaling in semidilute polymer solutions: a Monte Carlo test. *J. Phys. II* **1**, 37 (1991).
 - [87] Huang, C.-C. *et al.* Semidilute polymer solutions at equilibrium and under shear flow. *Macromolecules* **43**, 10107 (2010).
 - [88] In the following, we do not address the case of "toroidal" bottlebrushes [39], where the backbone becomes locally rod-like at very large values of N_{sc} and z . However, we discuss aspects of this case at the beginning of the Methods section.
 - [89] See also discussion above Eq. (14), where we derive this result using scaling arguments.